Adsorption and Reactions of $ClCH_2CH_2OH$ on Clean and Oxygen-Precovered Cu(100): Experimental and Computational Studies

Tao-Wei Fu, Yung-Hsuan Liao, Chia-Yuan Chen, Pei-Teng Chang, Ching-Yung Wang, and Jong-Liang Lin*

Department of Chemistry, National Cheng Kung University 1, Ta Hsueh Road, Tainan, Taiwan 701, Republic of China

Received: May 4, 2005; In Final Form: August 18, 2005

Temperature-programmed reaction/desorption, reflection−absorption infrared spectroscopy, and density functional theory calculations have been employed to investigate the adsorption and thermal reactions of $ClCH_2CH_2OH$ on clean and oxygen-precovered Cu(100) surfaces. On Cu(100), $ClCH_2CH_2OH$ is mainly adsorbed reversibly. The $ClCH_2CH_2OH$ molecules at a submonolayer coverage can change their orientation with increasing temperature. However, on oxygen-precovered Cu(100), all of the adsorbed $ClCH_2CH_2OH$ molecules below 0.5 langmuir exposures completely dissociate to generate ethylene and acetaldehyde via the intermediate of $ClCH_2CH_2O-$. The computational studies predict that the $ClCH_2CH_2O-$ is most likely to be adsorbed at the 4-fold hollow sites of Cu(100), with its C−O bond only slightly titled away from the surface normal and with a gauche conformation with respect to the C−C bond. The hollow-site $ClCH_2CH_2O-$ has an adsorption energy that is 4.4 and 19.2 kcal·mol^{-1} lower than that of the $ClCH_2CH_2O-$ bonded at the bridging and atop sites, respectively. No significant effect of precovered oxygen on the $ClCH_2CH_2O-$ bonding geometry and infrared band frequencies has been observed, as compared with the case without oxygen.

Introduction

For straight chain alkyl chlorides on Cu(100), it is found that C−Cl dissociation does not occur until the chain length reaches seven carbons. On the basis of the desorption temperature of chloropropane, chlorobutane, chloropentane, and chlorohexane and the assumption of a preexponential factor of 10^{13} s^{-1} of first-order desorption kinetics, the heat of molecular adsorption is estimated to increase at a rate of 1.3 kcal·mol^{-1} per CH_2 group.[1] Chloroheptane decomposes on Cu(100), forming heptene at 250 K.[1] On Pd(111), chlorobutane is the shortest alkyl chloride to dissociate.[2] Chloromethane does not dissociate on Al(111) and Pt(111).[3,4] For ethanol on Cu(100), only a few percent of the adsorbed molecules at monolayer coverage can dissociate. However, ethanol readily decomposes by O−H bond scission on oxygen-precovered Cu(100) (O/Cu(100)) between 200 and 300 K, generating acetaldehyde as an end product.[5,6] Alcohol molecules decompose by O−H bond scission on a large number of clean transition metal surfaces, such as Fe(110),[7] Ni(110),[8] Ni(100),[9] Ru(0001),[10] Mo(100),[11] Mo(110),[12] Rh-(111),[13] Pd(111),[14] and Pt(111).[15]

In the study of $ClCH_2CH_2OH$, with two reactive centers of C−Cl and C−OH, on Cu(100) and O/Cu(100), we are interested in the bond dissociation of $ClCH_2CH_2OH$, in the surface intermediates and their bonding geometry, in the reaction products, and in the effect of oxygen present on Cu(100). These subjects depend on the interaction between these two active centers and their interactions with the surface. Various surface intermediates are possibly generated from $ClCH_2CH_2OH$ decomposition on Cu(100) and O/Cu(100), such as $ClCH_2CH_2O-$, $HOCH_2CH_2-$, $-CH_2CH_2O-$, $HOCH_2CH_2O-$, and $-OCH_2-CH_2O-$, which are determined by the C−Cl and O−H bond dissociation temperatures. Studies of these intermediates are important in understanding the mechanisms of catalytic systems. Temperature-programmed reaction/desorption (TPR/D) and reflection−absorption infrared spectroscopy (RAIRS) have been employed to study the surface desorption and reactions. A program based on density functional theory (DFT) has been implemented to assist in the infrared analysis and in the prediction of the adsorption geometries for the surface intermediates generated from $ClCH_2CH_2OH$ decomposition. It is found that only a small percentage of a monolayer $ClCH_2CH_2OH$ dissociates on Cu(100), generating C_2H_4 at 302 K, in contrast to the $ClCH_2CH_2OH$ monolayer desorption at 213 K. The orientation of $ClCH_2CH_2OH$ molecules in the adsorption layer on Cu(100) may vary with the surface temperature. The reactions of $ClCH_2CH_2OH$ on O/Cu(100) at exposures ≤ 1 langmuir (1 L = 10^{-6} Torr·s) have been reported.[16] In the present research, the $ClCH_2CH_2OH$ exposure is extended to multilayer coverages. The RAIRS indicates that $ClCH_2CH_2OH$ dissociates on O/Cu(100) at 180 K, and the DFT calculations of infrared bands confirm the formation of a $ClCH_2CH_2O-$ surface intermediate. This intermediate is predicted to be adsorbed at a 4-fold hollow site. TPR/D shows that the decomposition of $ClCH_2CH_2O-$ evolves ethylene and acetaldehyde at temperatures higher than 275 K.

Experimental Section

All of the experiments were performed in an ultrahigh vacuum (UHV) apparatus equipped with an ion gun for sputtering, a differentially pumped mass spectrometer for TPR/D, four-grid spherical retarding field optics for low energy electron diffraction and Auger electron spectroscopy, and a Fourier transform infrared (FTIR) spectrometer for RAIRS. The chamber was evacuated by a turbomolecular pump and an ion pump to a base pressure of approximately 3×10^{-10} Torr. The quadrupole mass spectrometer used for the TPR/D study was capable of detecting

* Corresponding author. E-mail: jonglin@mail.ncku.edu.tw.

10.1021/jp052309g CCC: $30.25
Published on Web 09/20/2005

ions in the 1−300 amu range and of being multiplexed to acquire up to 15 different masses simultaneously in a single desorption experiment. In TPR/D experiments, the Cu(100) surface was positioned ∼1 mm from an aperture, 3 mm in diameter, leading to the mass spectrometer and a heating rate of 2 K/s was used. In the RAIRS study, the IR beam was taken from a Bomem FTIR spectrometer and focused at a grazing incidence angle of 85°, with respect to the surface normal, through a KBr window onto the Cu(100) in the UHV chamber. The reflected beam was then passed through a second KBr window and refocused on a mercury cadmium telluride detector. The entire beam path was purged with a Balston air scrubber for carbon dioxide and water removal. All of the IR spectra were taken at a temperature of about 115 K, with 800−1500 scans, and a 4 cm^{-1} resolution. The presented spectra have been ratioed against the spectra of a clean Cu(100) surface recorded immediately before 2-chloroethanol dosing. The Cu(100) single crystal (1 cm in diameter) was mounted on a resistive heating element and could be cooled with liquid nitrogen to 110 K and heated to 1100 K. The surface temperature was measured by a chromel−alumel thermocouple inserted into a hole on the edge of the crystal. Cleaning of the surface by cycles of Ar^+ ion sputtering and annealing was done prior to each experiment until no impurities were detected by Auger electron spectroscopy. 2-Chloroethanol (99%) was purchased from Riedel-deHaen and subjected to several freeze−pump−thaw cycles. Oxygen (99.998%) was obtained from Matheson. The purity of $ClCH_2CH_2OH$ was checked by mass spectrometry. The gas manifold for 2-chloroethanol was conditioned by backfilling with saturated 2-chloroethanol vapor pressure overnight. Prior to dosing 2-chloroethanol into the chamber, the gas manifold and 2-chloroethanol itself in the liquid state were pumped for a while.

The oxidized Cu(100) surface was prepared by exposing a clean Cu(100) surface at 500 K to 30 L of O_2, similar to the preparation for oxidized Cu(100) used in Sexton's study of alcohol.[5] Atomic oxygen was present on the surface after the O_2 treatment, as verified by Auger electron spectroscopy and electron energy loss spectroscopy. It was estimated that the oxygen coverage for the oxidized Cu(100) used in this study was ∼0.2 oxygen atoms per Cu atom (θ_o = ∼0.2).[17] The previous study showed that a long range order started to develop at $\theta_o = 0.34$ and a $(\sqrt{2} \times 2\sqrt{2})$R45° structure was formed at a saturation coverage of $\theta_o = 0.48$.[17]

In our calculations, the infrared spectra of $ClCH_2CH_2OH$ and $ClCH_2CH_2O-$ as well as the bonding geometries and relative energies of $ClCH_2CH_2O-$ at different sites on Cu(100) were obtained by running a Cerius^2-DMol^3 module,[18] based on density functional theory,[19] in which a double-numerical quality basis set with polarizations, except 2p for hydrogen, and Perdew−Wang functional (PWC) for exchange and correlation were used. The double-numerical quality basis sets with polarizations were comparable to 6-31G** sets. However, the numerical basis set was much more accurate than a Gaussian basis set of the same size. The calculations were spin-unrestricted and did not include relativistic effects for the core electrons. Two-point frequency calculation with an integration accuracy of 10^{-6} were performed on fully optimized structures of $ClCH_2CH_2OH$ and $ClCH_2CH_2O-$.

Results and Discussion

Temperature-Programmed Reaction/Desorption of $ClCH_2CH_2OH$ on Cu(100). A multiple-ion TPR/D survey shows three desorption maxima at 185, 213, and 302 K, following $ClCH_2CH_2OH$ adsorption up to 15 L on Cu(100) at 115 K. The first two states are due to $ClCH_2CH_2OH$ molecular desorption from multilayer and monolayer, respectively, in contrast to the C_2H_4 desorption at 302 K. Figure 1 illustrates the exposure-dependent $ClCH_2CH_2OH$ desorption represented by the CH_2OH^+ (m/z = 31) ion. At exposures ≤2 L, the highest $ClCH_2CH_2OH$ desorption rate appears at 213 K. However, as shown in the 0.1 L trace, there is a small desorption feature at ∼250 K, which is likely due to the $ClCH_2CH_2OH$ molecules being more strongly adsorbed at defect sites. For $ClCH_2CH_2OH$ exposures higher than 2 L, the 213 K peak gets saturated and a low temperature desorption state appears at ∼185 K, which is attributed to $ClCH_2CH_2OH$ multilayer desorption. Therefore, 2.0 L renders a monolayer coverage on a clean Cu(100) surface, that is, a saturated first layer coverage. In the inset of Figure 1, the linearly increased $ClCH_2CH_2OH$ desorption yield versus exposure suggests that $ClCH_2CH_2OH$ molecules are reversibly adsorbed within experimental error. However, there is a small amount C_2H_4 production confirmed by the $C_2H_3^+$ ion, as shown in the TPR/D spectra of Figure 2. In Figure 2, except for the 180 and 213 K peaks originated from $ClCH_2CH_2OH$ desorption, a new species is desorbed at 302 K and is identified to be C_2H_4 by the fragmentation pattern. Compared to the case of 0.5 L of $ClCH_2CH_2OH$ on O/Cu(100) (shown later) in which the $ClCH_2CH_2OH$ completely decomposes, the C_2H_4 amount from 2 L of $ClCH_2CH_2OH$ on Cu(100) is 4% of that from 0.5 L of $ClCH_2CH_2OH$ on O/Cu(100).

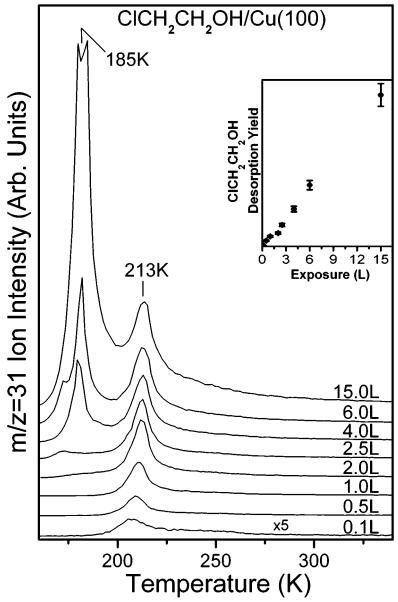

Figure 1. Temperature-programmed desorption spectra of a Cu(100) surface after dosing $ClCH_2CH_2OH$ at different exposures. The $ClCH_2CH_2OH$ desorption is represented by the CH_2OH^+ (m/z = 31) fragment. The 0.1 L trace is multiplied by a factor of 5. The inset shows the $ClCH_2CH_2OH$ desorption yield vs exposure.

Reflection−Absorption Infrared Spectroscopy of $ClCH_2CH_2OH$ on Cu(100). Figure 3a shows the infrared spectrum taken after the adsorption of 4 L of $ClCH_2CH_2OH$ on Cu(100) at 115 K. Note that a 4 L $ClCH_2CH_2OH$ exposure renders a coverage of two monolayers. The infrared bands appear at 750, 850, 942, 1035, 1084, 1164, 1241, 1301, and 1436 cm^{-1}. A number of $ClCH_2CH_2OH$ infrared studies regarding the absorption bands, vibrational mode assignment, conformational stability, and transition between the conformers have been reported.[20−29] In Table 1, the observed frequencies in Figure 3a are compared to those of $ClCH_2CH_2OH$ measured in the gas state and to the calculated bands for three different $ClCH_2CH_2OH$ conformers (Gg′, Tg, and Tt) in the framework of density functional theory.

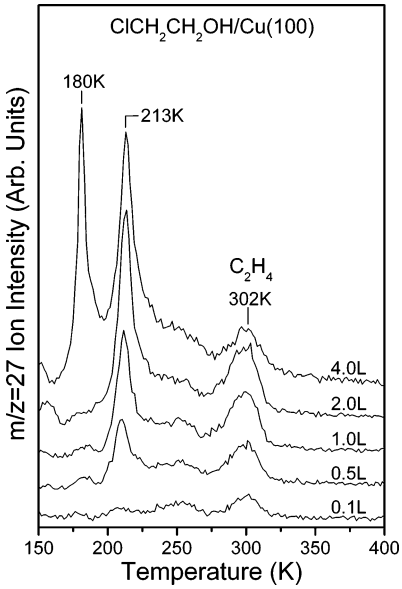

Figure 2. Temperature-programmed reaction/desorption spectra of a Cu(100) surface after dosing $ClCH_2CH_2OH$ at different exposures. The 180 and 213 K peaks are due to $ClCH_2CH_2OH$ desorption, in addition to C_2H_4 desorption at 302 K.

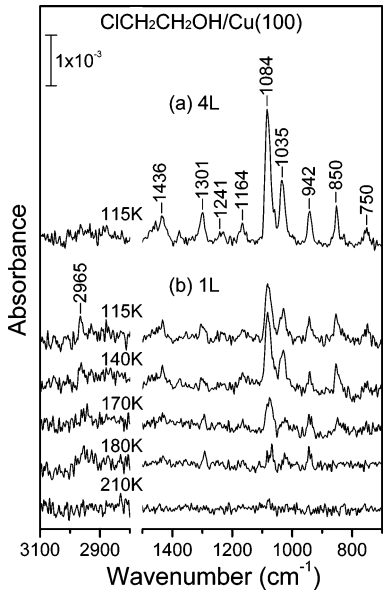

Figure 3. Reflection−absorption infrared spectrum of 4 L of $ClCH_2CH_2OH$ adsorbed on Cu(100) at 115 K and reflection−absorption infrared spectra taken after exposing 1 L of $ClCH_2CH_2OH$ to Cu(100) at 115 K and flashing the surface to the indicated temperatures.

The structures of the three $ClCH_2CH_2OH$ conformers are displayed in Figure 4. The G and T represent gauche and trans $ClCH_2CH_2OH$ forms, respectively, with respect to the C−C bond, in contrast to the g and t with respect to the C−O bond. Note that no scaling factor has been used for these computational frequencies and that the mode assignments are based on the animated vibrations of the corresponding bands. In the following analysis, the terms gauche and trans are used for the conformers with respect to the C−C bond. The infrared bands of $ClCH_2CH_2OH$ (Gg′, Tg, and Tt) have been predicted by ab initio calculation utilizing the MP2/6-31G* basis set.[20] Our calculated frequencies based on the local DFT method are basically consistent with this previous theoretical report and with the measured gaseous $ClCH_2CH_2OH$ infrared bands, as shown in Table 1. Accordingly, the present density functional calculations can reliably assist not only in the vibrational mode assignments for the conformers of the adsorbed $ClCH_2CH_2OH$ but also in the analysis of the $ClCH_2CH_2OH$ surface reaction pathways through surface intermediate investigation. Gg′ is the most stable conformer of $ClCH_2CH_2OH$ and is the only form present in the crystal.[20] However, the vapor and liquid phases contain the Gg′, Tt, and Tg forms. In the $ClCH_2CH_2OH$ vapor state, the number ratio of gauche/trans is ∼3 at 25 °C.[28] The observed bands in the 4 L $ClCH_2CH_2OH$ spectrum of Figure 3 are similar to those of gaseous $ClCH_2CH_2OH$, indicating that $ClCH_2CH_2OH$ is molecularly adsorbed on Cu(100) at 115 K. Furthermore, the gauche and trans $ClCH_2CH_2OH$ coexist on the surface, judged by the mode assignments. The 750 cm^{-1} band is due to the C−Cl stretching vibration of trans $ClCH_2CH_2OH$, and the 850 cm^{-1} one is due to the rocking vibration of gauche $ClCH_2CH_2OH$. The C−Cl stretching band of gauche $ClCH_2CH_2OH$ is not measured because of our instrumental cutoff frequency at 700 cm^{-1}. Figure 3b shows the temperature-dependent spectra of 1 L of $ClCH_2CH_2OH$ on Cu(100). The 115 K spectrum is similar to that of 4 L in terms of band frequencies and relative intensities, indicating that $ClCH_2CH_2OH$ molecules with gauche and trans forms are present on the surface at half monolayer coverage. The spectral feature starts to change after heating to 170 K. In the 180 K spectrum, the 750 and 850 cm^{-1} bands are not observed and the intensities of the 1035 and 1084 cm^{-1} bands decrease significantly. Because no new bands appear, this spectral change is not attributed to $ClCH_2CH_2OH$ decomposition. Although the possibility of $ClCH_2CH_2OH$ desorption leading to partial decrease of peak intensities at 180 K cannot be completely ruled out, this effect may not be significant. Note that the onset temperature of $ClCH_2CH_2OH$ desorption at a 1 L exposure is 190 K, as revealed in the TPR/D study. Therefore, the infrared change in intensity at 180 K is not attributed to $ClCH_2CH_2OH$ desorption but mainly to the change of $ClCH_2CH_2OH$ adsorption orientation. In the 180 K spectrum, the 942 cm^{-1} C−C stretching band of the Gg′ form is comparable to that observed in the 115 and 140 K spectra. However, the 850 cm^{-1} *CH_2 rocking band of Gg′ $ClCH_2CH_2OH$ is absent in the 180 K spectrum. Note that *C denotes the carbon which is bonded to the chlorine of $ClCH_2CH_2OH$. The combined RAIRS and TPD results suggest that the orientation of the adsorbed Gg′ form varies due to the surface heating. Figure 5 shows a possible orientation change of the adsorbed gauche $ClCH_2CH_2OH$ from 115 to 180 K that explains the change of relative band intensities. The Figure 5b orientation can be achieved simply by rotating the Figure 5a molecule around the C−C axis. The band intensity of the C−C stretching mode (942 cm^{-1}) is not expected to be changed, according to the surface dipole selection rule of RAIRS, because the angle between the C−C bond and the surface is invariant. However, due to the rotation, the C−O bond becomes much more parallel to the surface, as shown in Figure 5b. Therefore, the C−O stretching intensity of 1084 cm^{-1} is expected to be largely reduced in the Figure 5b orientation. A similar situation occurs in the case of the *CH_2 rocking mode. The dynamic dipole moment of *CH_2 rocking vibration in the surface normal direction for Figure 5b is much smaller than that for Figure 5a, leading to the disappearance of the 850 cm^{-1} band in 180 K spectrum of Figure 3b. The bands of trans $ClCH_2CH_2OH$ on Cu(100) are also affected by the increase of surface temperature. In Figure 3b, the 750 cm^{-1} C−Cl stretching band of trans $ClCH_2CH_2OH$ is no longer observed at 180 K, suggesting also the change of adsorption orientation. As the adsorbed trans $ClCH_2CH_2OH$ molecules adopt an orientation with their Cl−C−C−O backbone more parallel to the surface,

TABLE 1: Comparison of the Observed and Calculated Infrared Frequencies (cm^{-1}) of 2-Chloroethanol

		local DFT calculation of $ClCH_2CH_2OH$ (this work)[c,d]		
4 L of $ClCH_2CH_2OH$ on Cu(100), 115 K (this work)[a]	$ClCH_2CH_2OH$(g)[b]	Gg′	Tg	Tt
	673	658 ν(C−Cl)		
750 w	765		754 ν(C−Cl)	777 ν(C−Cl)
850 w	853	855 ρ(*CH_2)	768 ρ(*CH_2) + ρ(CH_2)	812 ρ(*CH_2)
942 w	933	931 ν(C−C)		
			1003 ρ(CH_2) + tw(*CH_2)	991 ν(C−C)
1035 m	1042	1033 tw(*CH_2)	1055 ν(C−C)	1035 tw(*CH_2)
	1056			
1084 s	1078	1102 ν(C−O)	1085 ν(C−O)	1120 ν(C−O)
1164 w	1177	1174 tw(*CH_2) + tw(CH_2)	1107 tw(*CH_2) + tw(CH_2)	1186 tw(*CH_2) + tw(CH_2)
	1201	1186 tw(*CH_2) + tw(CH_2)	1227 ω(*CH_2)	1227 ω(*CH_2) + ω(CH_2)
1241 w		1267 ω(*CH_2)	1262 tw(*CH_2) + tw(CH_2)	1270 tw(*CH_2) + tw(CH_2)
1301 w	1292			1288 ω(*CH_2) + ω(CH_2)
	1354	1342 tw(CH_2)	1338 bending(COH)	
	1395	1378 ω(CH_2) + bending(COH)	1361 ω(CH_2) + bending(COH)	1422 ω(CH_2) + bending(COH)
1436 w	1436	1414 δ(*CH_2)	1428 δ(*CH_2)	1446 δ(*CH_2)
	1455	1442 δ(CH_2)	1451 δ(CH_2)	1462 δ(CH_2)
	2844			2864 ν_s(CH_2)
	2933	2903 $\nu_s$$CH_2$)	2934 ν_s(CH_2)	2910 ν_a(CH_2)
				2916 ν_s(*CH_2)
	2969	2996 ν_a(CH_2) + ν_s(*CH_2)	2992 ν_s(*CH_2)	2983 ν_a(*CH_2)
	3013	3007 ν_s(*CH_2) + ν_a(CH_2)	3033 ν_a(CH_2)	
		3077 ν_a(*CH_2)	3069 ν_a(*CH_2)	
		3552 ν(O−H)	3627 ν(O−H)	3517 ν(O−H)

[a] w, weak; m, medium; s, strong. [b] From ref 20. [c] An asterisk denotes the CH_2 that is bonded to Cl. [d] ρ, rocking; tw, twisting; ω, wagging; δ, scissoring; ν_s, symmetric stretching; ν_a, antisymmetric stretching.

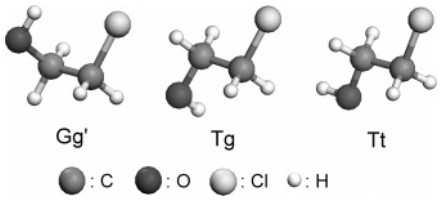

Figure 4. Three conformational isomers of $ClCH_2CH_2OH$.

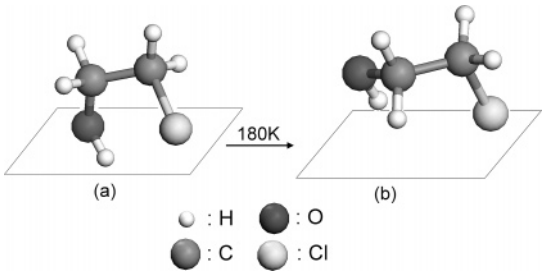

Figure 5. A possible change in the orientation of adsorbed $ClCH_2CH_2OH$ on Cu(100).

their C−O and C−Cl stretching intensities are expected to be reduced. It should be stressed that Figure 5 only demonstrates a plausible orientation change with temperature. The real orientation should be studied with other surface analytical techniques. In Figure 3b, as the surface is further heated to 210 K, no infrared bands are detected, which is consistent with the $ClCH_2CH_2OH$ desorption observed in the TPR/D study.

Temperature-Programmed Reaction/Desorption of $ClCH_2CH_2OH$ on O/Cu(100). As oxygen atoms are present on Cu(100), the binding strength and thermal stability of $ClCH_2CH_2OH$ are perturbed. Figure 6 shows the spectra of $ClCH_2CH_2OH$ desorption, represented by the CH_2OH^+ ion, following $ClCH_2CH_2OH$ adsorption at different exposures. For an exposure $\leq$0.5 L, $ClCH_2CH_2OH$ desorption is not found, indicating its decomposition on O/Cu(100). $ClCH_2CH_2OH$ dissociates on O/Cu(100) between 170 and 220 K at a 0.5 L exposure.[16] As the exposure is increased to 1 L, the $ClCH_2CH_2OH$ desorption appears at

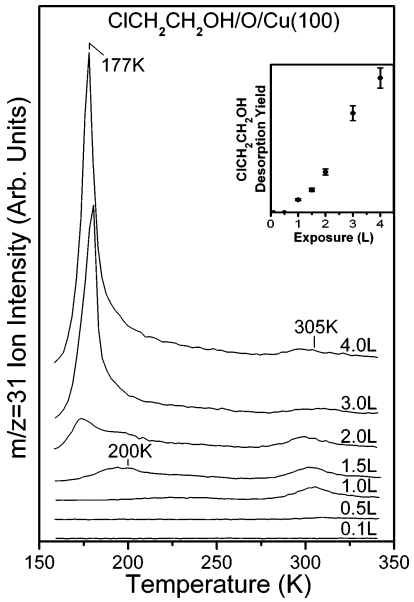

Figure 6. Temperature-programmed desorption spectra of a Cu(100) surface after dosing $ClCH_2CH_2OH$ at different exposures. The $ClCH_2CH_2OH$ desorption is represented by the CH_2OH^+ (m/z = 31) fragment. The inset shows the $ClCH_2CH_2OH$ desorption yield vs exposure.

305 K. There are additional low-temperature desorption states at higher exposures. The inset of Figure 6 shows the $ClCH_2CH_2OH$ desorption yield as a function of exposure. Figure 7 shows the TPR/D spectra for the evolution of C_2H_4, represented by the $C_2H_3^+$ ion, and CH_3CHO, represented by the CH_3CO^+ ion, from $ClCH_2CH_2OH$ decomposition on O/Cu(100). H_2O is also generated and desorbed at ~200 K (Figure 8).

Reflection−Absorption Infrared Spectroscopy of $ClCH_2CH_2OH$ on O/Cu(100). Figure 9 shows the temperature-dependent infrared spectra taken after the adsorption of 4 L of $ClCH_2CH_2OH$ on O/Cu(100) at 115 K. The 115 K spectrum is similar to that of 4 L on Cu(100) at this temperature and is attributed to adsorbed $ClCH_2CH_2OH$. The 150 K spectrum

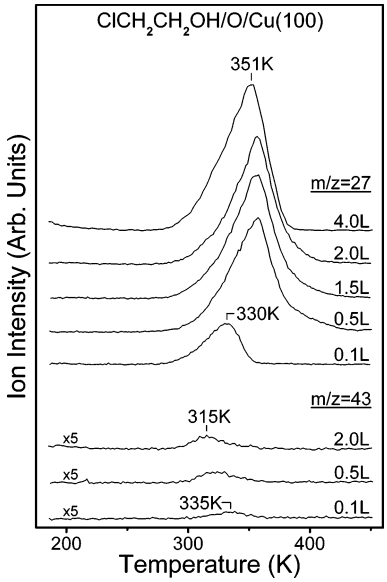

Figure 7. Temperature-programmed reaction/desorption spectra of a O/Cu(100) surface after dosing the indicated $ClCH_2CH_2OH$ exposures at 115 K, collected for the $C_2H_3^+$ and $C_2H_3O^+$ ions, representative of C_2H_4 and CH_3CHO desorption, respectively.

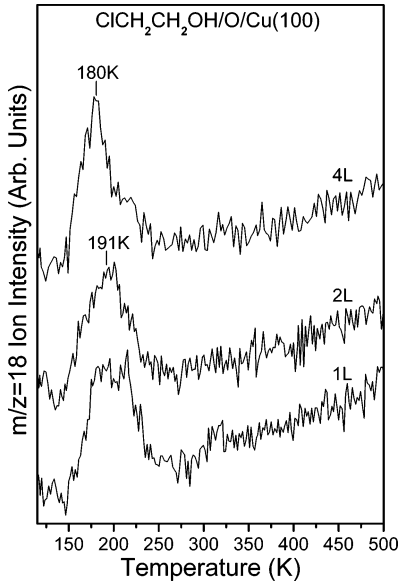

Figure 8. Temperature-programmed reaction/desorption spectra of H_2O evolution after dosing 1, 2, and 4 L of $ClCH_2CH_2OH$ on O/Cu(100) at 115 K.

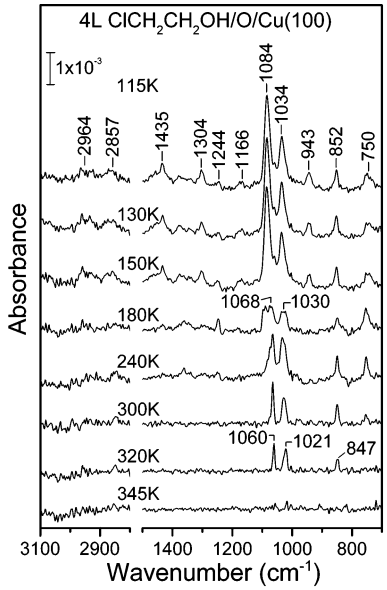

Figure 9. Reflection−absorption infrared spectra taken after exposing 4 L of $ClCH_2CH_2OH$ to O/Cu(100) at 115 K and flashing the surface to the indicated temperatures.

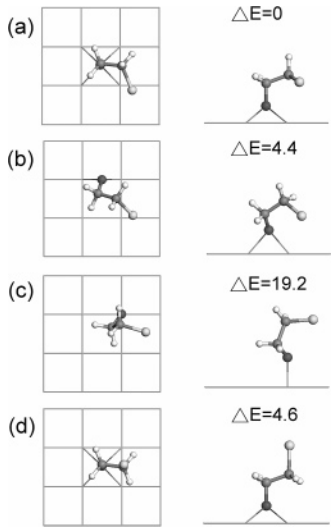

Figure 10. Optimized structures, with top and side views, of $ClCH_2CH_2O-$ adsorbed at the hollow (a), bridging (b), and atop (c) sites of Cu(100), respectively. Part d shows the $ClCH_2CH_2O-$ structure with a trans conformation relative to the C−C bond. ΔE is the energy difference in kilocalories per mole for each structure relative to part a.

resembles the 115 K one. However, the spectral feature changes at 180 K, with the obvious decrease in intensity of the 1034 and 1084 cm^{-1} bands. This corresponds to the multilayer $ClCH_2CH_2OH$ desorption peaked at 177 K, as revealed in Figure 6. Furthermore, a new band at 1068 cm^{-1} appears, suggesting that decomposition of $ClCH_2CH_2OH$ proceeds together with desorption at 180 K. After heating the surface to 240 K, the peaks at 852, 1030, and 1068 cm^{-1} grow, as compared to the 180 K spectrum. The 1084 cm^{-1} band continues to decrease and becomes a shoulder of the 1068 cm^{-1} band. In the 300 K spectrum, the 1084 cm^{-1} band disappears, showing further desorption and/or decomposition of $ClCH_2CH_2OH$. As the surface is heated to 320 K, only three bands at 847, 1021, and 1060 cm^{-1} are observed. These three bands are no longer detected at 345 K which is the desorption temperature of C_2H_4 and CH_3CHO, as shown in Figure 7. Therefore, the species responsible for the bands of 847, 1021, and 1060 cm^{-1} should be the intermediate for the production of C_2H_4 and CH_3CHO. Temperature-dependent infrared investigations for 0.5, 1, and 2 L of $ClCH_2CH_2OH$ on O/Cu(100) were also carried out and showed a similar changing behavior. The desorption products observed in the $ClCH_2CH_2OH$ TPR/D studies can show some clues for the $ClCH_2CH_2OH$ decomposition pathway and the surface intermediates generated on O/Cu(100). The H_2O desorption at ~200 K indicates the rupture of the O−H bond of $ClCH_2CH_2OH$. The C_2H_4 desorption indicates that the surface intermediate for this product contains the $-CH_2CH_2-$ moiety. However, surface species such as $-OCH_2CH_2O-$ and $-CH_2CH_2O-$, which meet the TPR/D arguments, cannot account for the three bands at 847, 1021, and 1060 cm^{-1}. It has been reported that $-OCH_2CH_2O-$ on O/Cu(100) has two vibrational absorptions at 880 and 1090 cm^{-1}.[30] $-CH_2CH_2O-$ on O/Cu(100), generated from 2.5 L $BrCH_2CH_2OH$ dissociative adsorption, shows two strong bands of 1002 and 1059 cm^{-1} at 260

TABLE 2: Structural Parameters of $ClCH_2CH_2O-$ Adsorbed at Hollow, Bridging, and Atop Sites of Cu(100) (Figure 10a−c) and at Hollow Sites on O/Cu(100) (Figure 11)[a]

without O			with O
hollow	bridging	atop	hollow
d(C−Cl) = 1.80	d(C−Cl) = 1.83	d(C−Cl) = 1.79	d(C−Cl) = 1.80
d(C−C) = 1.49	d(C−C) = 1.49	d(C−C) = 1.50	d(C−C) = 1.49
d(C−O) = 1.42	d(C−O) = 1.39	d(C−O) = 1.36	d(C−O) = 1.42
$\theta(COS_N)$ = 3.6°	$\theta(COS_N)$ = 43.6°	$\theta(COS_N)$ = 52.2°	$\theta(COS_N)$ = 4.1°
$\theta(CCS_N)$ =69.3°	$\theta(CCS_N)$ = 56.8°	$\theta(CCS_N)$ =21.1°	$\theta(CCS_N)$ =71.4°
$\theta(CClS_N)$ =75.5°	$\theta(CClS_N)$ = 59.4°	$\theta(CClS_N)$ =93.8°	$\theta(CClS_N)$ =76.3°
θ(OCC) =110.7°	θ(OCC) =113.4°	θ(OCC) =109.7°	θ(OCC) =111.0°
θ(CCCl) =110.4°	θ(CCCl) =110.9°	θ(CCCl) =110.8°	θ(CCCl) =110.4°
h(O) = 1.068	h(O) = 1.504	h(O) = 1.849	h(O) = 1.067
			h(O*) = 0.587

[a] d, bond length (Å); θ, bond angle; h, height from the Cu surface (Å); S_N, surface normal; O*, adsorbed oxygen atom.

K.[31] After exclusion of the possibility of $-OCH_2CH_2O-$ and $-CH_2CH_2O-$, the most likely intermediate is $ClCH_2CH_2O-$. To provide further support for the formation of this intermediate and to understand its adsorption geometry, density functional theory calculations have been employed to predict the $ClCH_2CH_2O-$ infrared band frequencies and relative energies at different surface sites.

Theoretical Analysis of the Infrared Bands and Adsorption Geometry of $ClCH_2CH_2O-$. In our calculations for the adsorption geometry of $ClCH_2CH_2O-$ on Cu(100), a slab of 16 Cu atoms fixed at their lattice positions was used. Figure 10a shows the most stable adsorption structure of $ClCH_2CH_2O-$ (top and side views), obtained by minimizing the total energy. In the optimizing process, all of the bond lengths and angles of $ClCH_2CH_2O-$, including the C−Cu bond, were allowed to vary. Detailed structure information is shown in Table 2. There are several important structure features in this bonding geometry. $ClCH_2CH_2O-$ is adsorbed at the 4-fold hollow site of Cu(100). The C−O bond of the $ClCH_2CH_2O-$ is tilted away from the surface normal by 3.6°. The C−Cl bond of the $ClCH_2CH_2O-$ is close to the surface. The $ClCH_2CH_2O-$ basically has a gauche conformation with respect to the C−C bond. The optimized bonding geometries and total energies of $ClCH_2CH_2O-$ bonded at bridging and atop sites were also calculated in order to compare to the hollow-site case. In these calculations, $ClCH_2CH_2O-$ was fixed at a bridging or atop site; however, all of the bond lengths and angles, including the distance between the O atom and the copper surface, were variable. The bonding structures of $ClCH_2CH_2O-$ at bridging and atop sites of Cu(100) and their energies relative to the case of $ClCH_2CH_2O-$ at hollow sites are shown in Figure 10b and c and Table 2. The $ClCH_2CH_2O-$ bonded at these specific surface sites basically has a gauche conformation. The bridging and atop $ClCH_2CH_2O-$ have adsorption energies 4.4 and 19.2 kcal·mol^{-1} higher than the case of hollow-site adsorption, respectively. As $ClCH_2CH_2O-$ is adsorbed with the trans conformation, our calculations predict that it has a higher adsorption energy than the gauche form. Figure 10d shows the optimized geometry of $ClCH_2CH_2O-$, with the trans conformation, at the hollow site and its relative energy. The trans $ClCH_2CH_2O-$ has an energy 4.6 kcal·mol^{-1} higher than the gauche $ClCH_2CH_2O-$ bonded at the hollow site of Cu(100).

Table 3 compares the calculated infrared band frequencies and the corresponding vibrational modes for the $ClCH_2CH_2O-$ adsorbed at hollow, bridging, and atop sites, as shown in Figure 10. The calculated C−Cl stretching band of the trans $ClCH_2CH_2O-$ is 763 cm^{-1} which is close to that of trans $ClCH_2CH_2OH$ and is much larger than those of gauche $ClCH_2CH_2O-$ listed in Table 3. The experimental bands observed in the case of 4 L $ClCH_2CH_2OH$ adsorption on O/Cu(100) followed by brief annealing to 320 K are also shown in the first column of Table 3 for comparison and for the support of $ClCH_2CH_2O-$ generation from $ClCH_2CH_2OH$ thermal decomposition. It is found that the 847, 1021, and 1060 cm^{-1} bands are closely similar to the calculated band frequencies of gauche $ClCH_2CH_2O-$ bonded at the hollow site of Cu(100), with a wavenumber difference $\leq$17 cm^{-1}. However, for the gauche $ClCH_2CH_2O-$ at bridging and atop sites, their calculated C−O and/or C−C stretching frequencies at 1102 and 1107 cm^{-1} are much larger than the observed 1060 cm^{-1} band. The trans $ClCH_2CH_2O-$ at the hollow site has no band near 847 cm^{-1}; therefore, it is not considered as the $ClCH_2CH_2OH$ reaction intermediate with a right conformation. Note that the 4-fold hollow sites of Cu(100) are predicted to be the most stable position for gauche $ClCH_2CH_2O-$ adsorption, which is consistent with the closely

TABLE 3: Comparison of the Observed and Calculated Infrared Frequencies (cm^{-1}) of $ClCH_2CH_2O-$ on Cu(100)

	DFT calculation of $ClCH_2CH_2-$				
4 L of $ClCH_2CH_2OH$ on O/Cu(100), 320 K	Cu(100) hollow site, gauche (Figure 10a)	Cu(100) bridging site, gauche (Figure 10b)	Cu(100) atop site, gauche (Figure 10c)	Cu(100) hollow site, trans (Figure 10d)	O/Cu(100) hollow site, gauche (Figure 11)
	639 ν(C−Cl)	563 ν(C−Cl)	674 ν(C−Cl)	763 ν(C−Cl) 778 $\rho(CH_2) + \rho(*CH_2)$	630 ν(C−Cl) + ω(*CH_2)
847	833 in plane CCO bending + ρ(*CH_2)	846 in plane CCO bending + ρ(*CH_2)	864 in plane CCO bending + ρ(*CH_2)		840 in plane CCO bending
	929 $\rho(CH_2) + \omega(*CH_2)$	917 $\rho(CH_2) + \omega(*CH_2)$	922 $\rho(CH_2) + \omega(*CH_2)$		924 $\rho(CH_2)$
				961 ν(C−O)	
1021	1004 ν(C−O)	1001 tw(*CH_2) + $\rho(CH_2)$	1025 ν(C−C)	1015 tw(*CH_2) + $\rho(CH_2)$	1003 ν(C−O)
1060	1061 ν(C−O) + ν(C−C)	1102 ν(C−O) + ν(C−C)	1107 ν(C−O)	1078 ν(C−C)	1069 ν(C−O) + ν(C−C)
	1162 tw(*CH_2) + tw(CH_2)	1141 tw(*CH_2) + tw(CH_2)	1148 tw(*CH_2) + tw(CH_2)	1142 tw(*CH_2) + tw(CH_2)	1160 tw(*CH_2) + tw(CH_2)
	1208 tw(CH_2) + ν(C−C)	1201 ω(*CH_2) + tw(CH_2)	1201 tw(*CH_2) + tw(CH_2)	1208 ω(*CH_2) + ω(CH_2)	1211 tw(CH_2) + ω(*CH_2)
	1270 ω(*CH_2) + tw(CH_2)	1243 ω(*CH_2) + tw(CH_2)	1259 ω(*CH_2)	1241 tw(CH_2) + tw(*CH_2)	1262 ω(*CH_2)
	1321 ω(CH_2)	1315 ω(CH_2)	1285 ω(CH_2)	1315 ω(CH_2) + ω(*CH_2)	1331 ω(CH_2)
	1381 δ(*CH_2)	1385 δ(CH_2)	1376 δ(CH_2)	1412 δ(*CH_2)	1391 δ(*CH_2)
	1419 δ(CH_2)	1397 δ(*CH_2)	1402 δ(*CH_2)	1440 δ(CH_2)	1405 δ(CH_2)
	2915 ν_s(CH_2)	2657 ν_s(CH_2)	2697 ν_s(CH_2)	2938 ν_s(*CH_2)	2913 ν_s(CH_2)
	2926 ν_s(*CH_2)	2884 ν_a(CH_2)	2746 ν_a(CH_2)	2949 ν_s(CH_2)	2931 ν_s(*CH_2)
	2975 ν_a(CH_2)	2998 ν_s(*CH_2)	2988 ν_s(*CH_2)	2994 ν_a(CH_2)	2985 ν_a(CH_2)
	3038 ν_a(*CH_2)	3078 ν_a(*CH_2)	3061 ν_a(*CH_2)	3018 ν_a(*CH_2)	3038 ν_a(*CH_2)

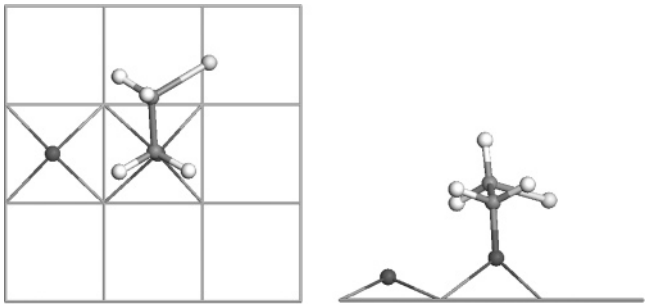

Figure 11. Optimized structure, with top and side views, of $ClCH_2CH_2O-$ adsorbed at the Cu(100) hollow site with an adjacent oxygen atom.

matched infrared bands obtained experimentally and theoretically, as shown in Table 3. In this $ClCH_2CH_2O-$ adsorption geometry, the three vibrational modes for 847, 1021, and 1060 cm^{-1} all have nonzero dynamic dipole moments perpendicular to the surface that allow the bands to be measured.

The effect of coadsorbed oxygen atoms on the $ClCH_2CH_2O-$ adsorption geometry and infrared absorption frequencies was investigated as well. The preferred oxygen adsorption site was first determined theoretically. It is found that an isolated oxygen atom bonded at the hollow site of Cu(100) has an energy 38.0 and 59.2 kcal·mol^{-1} lower than the one bonded at bridging and atop sites, respectively. The previous study reported that oxygen atoms were preferentially adsorbed on the hollow sites of Cu(100), using high-resolution electron energy-loss spectroscopy.[32] Therefore, in the investigation of the oxygen effect, the oxygen atoms are assumed to be bonded at the 4-fold hollow sites. Our theoretical calculations, through the search of the fully optimized bonding structure with the minimum total energy of $ClCH_2CH_2O-$ on O/Cu(100), predict that the most stable $ClCH_2CH_2O-$ adsorption position is the hollow site in the proximity of a hollow-site oxygen atom. The structure of the $ClCH_2CH_2O-$ bonded at a hollow site next to an atomic oxygen is shown in Figure 11. The calculated infrared bands and detailed structural information of the $ClCH_2CH_2O-$ are shown in the last columns of Tables 3 and 2, respectively. In both cases of hollow-site $ClCH_2CH_2O-$ with and without an adjacent oxygen atom, the theoretical results show similar infrared frequencies and adsorption geometries. On clean Cu(100), only a few percent of monolayer $ClCH_2CH_2OH$ decomposes, similar to the case of C_2H_5OH.[5,6] Most of the surface $ClCH_2CH_2OH$ molecules are desorbed at 213 K. Note that the C−Cl bond scission temperature of alkyl chlorides on Cu(100) is higher than 236 K.[1] It suggests that $ClCH_2CH_2OH$ dissociates via O−H bond scission preceding the C−Cl bond, generating C_2H_4 as a desorption product. In contrast to the case of $ClCH_2CH_2OH$, $BrCH_2CH_2OH$ (≤2 L) on Cu(100) dissociates at ∼190 K to generate $-CH_2CH_2O-$.[31] The bond energies of C−Br and C−Cl are approximately 70 and 85 kcal·mol^{-1}, respectively. Bromopropane decomposes readily on Cu(100) at 180 K, forming propyl groups on the surface.[1] The C−X bond energy is a dominant factor controlling the reaction pathways of XCH_2CH_2OH on Cu(100). The reactions of XCH_2CH_2OH (X = F, Cl, Br, and I) on Ru(111) have been investigated.[33] The reaction routes and product distribution are dependent on the nature of carbon−halogen bonds. $ClCH_2CH_2OH$ decomposes on Ru(111) to form CH_4, H_2, and CO_2. In the case $ClCH_2CH_2OH$/Cu(100), the C−C bond remains intact in the TPR/D studies. On O/Cu(100), $ClCH_2CH_2OH$ dissociates via O−H bond scission to form $ClCH_2CH_2O-$, as identified by the 180 K RAIR spectrum (Figure 9). The carbon−halogen effect is also seen in the case of O/Cu(100). $BrCH_2CH_2OH$ dissociates to form $-CH_2CH_2O-$ on O/Cu(100) at 115 K, although the O−H bonds of alcohol molecules break on O/Cu(100) between 200 and 300 K.[5,6]

In the present theoretical studies, it assists in the identification of $ClCH_2CH_2O-$ generated from decomposition on O/Cu(100) and provides the optimized geometry and the most probable adsorption site for this surface intermediate. The calculated difference in the energy for $ClCH_2CH_2O-$ adsorbed at specific surface sites also suggests the directional diffusion barriers that $ClCH_2CH_2O-$ moves on the surface. It is predicted that O and $ClCH_2CH_2O-$ are most likely to be adsorbed at the 4-fold hollow site of Cu(100). There is an implication in the decomposition of $ClCH_2CH_2O-$ on Cu(100). Because the hollow site is the most stable site for O adsorption with an energy 38.0 and 59.2 kcal·mol^{-1} lower than bridging and atop sites, respectively, from the thermodynamic point of view, $ClCH_2CH_2O-$ is likely to dissociate by breaking the C−Cl and C−O bonds to form C_2H_4 at the hollow site. However, dynamic investigations are needed to understand the reaction paths, especially in the transition state.

Conclusions

The combined results of RAIRS and TPR/D studies show that $ClCH_2CH_2OH$ on Cu(100) is mainly adsorbed reversibly, with a minor decomposition pathway to form ethylene. The molecular orientation of adsorbed $ClCH_2CH_2OH$ molecules can change with surface temperature. However, on oxygen-preadsorbed Cu(100), all of the $ClCH_2CH_2OH$ molecules below a 0.5 L exposure completely dissociate, forming ethylene and acetaldehyde. RAIRS and density functional theory calculations indicate that $ClCH_2CH_2OH$ decomposes on O/Cu(100) via a $ClCH_2CH_2O-$ intermediate, which is most likely to be adsorbed at the 4-fold hollow site. The computational study suggests that in the case of both O and $ClCH_2CH_2O-$ adsorbed at hollow sites next to each other, $ClCH_2CH_2O-$ has a similar bonding geometry and infrared band frequencies to those of $ClCH_2CH_2O-$ in the absence of O.

Acknowledgment. The work was supported by the National Center for High-Performance Computing and the National Science Council of the Republic of China (NSC 93-2113-M-006-010).

References and Notes

(1) Lin, J.-L.; Bent, B. E. *J. Phys. Chem.* **1992**, *96*, 8529.
(2) Zhou, G.; Gellman, A. J. *J. Catal.* **2000**, *194*, 233.
(3) Jo, S. K.; Zhu, X.-Y.; Lennon, D.; White, J. M. *Surf. Sci.* **1991**, *241*, 231.
(4) Chen, J. G.; Beebe, T. P., Jr.; Crowell, J. E.; Yates, J. T., Jr. *J. Am. Chem. Soc.* **1987**, *109*, 1726.
(5) Sexton, B. A. *Surf. Sci.* **1979**, *88*, 299.
(6) Bowker, M.; Madix, R. J. *Surf. Sci.* **1982**, *116*, 549.
(7) McBreen, P. H.; Erley, W.; Ibach, H. *Surf. Sci.* **1983**, *133*, L469.
(8) Richter, L. J.; Ho, W. *J. Chem. Phys.* **1985**, *83*, 2569.
(9) Gleason, N.; Guevremont, J.; Zaera, F. *J. Phys. Chem. B* **2003**, *107*, 11133.
(10) Barros, R. B.; Garcia, A. R.; Ilharco, L. M. *J. Phys. Chem. B* **2001**, *105*, 11186.
(11) Miles, S. L.; Bernasek, S. L.; Gland, J. L. *J. Phys. Chem.* **1983**, *87*, 1626.
(12) Wiegand, B. C.; Uvdal, P. E.; Serafin. J. G.; Friend, C. M. *J. Am. Chem. Soc.* **1991**, *113*, 6686.
(13) Berko, A.; Tarnoczi, T. I.; Solymosi, F. *Surf. Sci.* **1987**, *189*, 238.
(14) Davis, J. L.; Barteau, M. A. *Surf. Sci.* **1990**, *235*, 235.
(15) Sexton, B. A. *Surf. Sci.* **1981**, *102*, 271.
(16) Chang, P.-T.; Kuo, K.-H.; Shih, J.-J.; Chen, C.-Y.; Lin, J.-L. *Surf. Sci.* **2004**, *561*, 208.
(17) Wuttig, M.; Franchy, R.; Ibach, H. *Surf. Sci.* **1989**, *213*, 103.
(18) Delley, B. *J. Chem. Phys.* **2000**, *113*, 7756.
(19) *Density Functional Methods in Chemistry*; Labanowski, J. K., Andzelm, J. W., Eds.; Springer-Verlag: New York, 1991.

(20) Durig, J. R.; Zhou, L.; Gounev, T. K.; Klaeboe, P.; Guirgis, G. A.; Wang, L.-F. *J. Mol. Struct.* **1996**, *385*, 7.
(21) Krueger, P. J.; Mettee, H. D. *Can. J. Chem.* **1964**, *42*, 326.
(22) Wyn-Jones, E.; Orville-Thomas, W. J. *J. Mol. Struct.* **1967**, *1*, 79.
(23) Barnes, A. J.; Bentwood, R. M. *J. Mol. Struct.* **1984**, *112*, 31.
(24) Takeuchi, H.; Tasumi, M. *Chem. Phys.* **1987**, *70*, 275.
(25) Perttilla, M.; Murto, J.; Halonen, L. *Spectrochim. Acta* **1978**, *34A*, 469.
(26) Murto, J.; Rasanen, M.; Aspiala, A.; Homanen, L. *J. Mol. Struct.* **1983**, *92*, 45.
(27) Murto, J.; Rasanen, M.; Aspiala, A.; Lotta, T. *J. Mol. Struct.* **1984**, *108*, 99.
(28) Buckley, P.; Giguere, P. A.; Schneider, M. *Can. J. Chem* **1969**, *47*, 901.
(29) Davidovics, G.; Pourcin, J.; Monnier, M.; Verlaque, P.; Bodot, H.; Abouaf-Marquin, L.; Gauthier-Roy, B. *J. Mol. Struct.* **1984**, *39*, 116.
(30) Bryden, T. R.; Garrett, S. T. *J. Phys. Chem. B* **2001**, *105*, 9280.
(31) Chang, P.-T.; Shih, J.-J.; Kuo, K.-H.; Chen, C.-Y.; Fu, T.-W.; Shih, D.-L.; Liao, Y.-H.; Lin, J.-L. *J. Phys. Chem. B* **2004**, *108*, 13320.
(32) Ellis. T. H.; Kruus, E. J.; Wang, H. *J. Vac. Sci. Technol., A* **1993**, *11*, 2117.
(33) Brown, N. F.; Barteau, M. A. *J. Phys. Chem.* **1994**, *98*, 12737.